

Skin temperature perturbations induced by surface layer turbulence above a grass surface

Gabriel G. Katul,^{1,2} John Schieldge,³ Cheng-I Hsieh,¹ and Brani Vidakovic⁴

Abstract. High-frequency (5 Hz) atmospheric surface layer (ASL) turbulent velocity (u') and infrared skin temperature perturbations (T'_s) were measured above a grass-covered forest clearing and analyzed for cloud free conditions. These measurements were used to investigate mechanisms responsible for the production of large short-lived T'_s perturbations caused by rapid excursions in u' . To quantify the effects of u' on rapid surface cooling, wavelet spectra of u' and T'_s and cospectra of $u'T'_s$ were computed. The u' wavelet power spectra were then analyzed using *Townsend's* [1961, 1976] hypothesis. *Townsend's* hypothesis states that ASL eddy motion can be decomposed into an active component, which is a function of the ground shear stress (u_*) and height (z) above the zero plane displacement, and an inactive component, which is produced in the atmospheric boundary layer (ABL) outer region. A -1 power law in the u' power spectrum was used as a signature for inactive eddy motion. Therefore the -1 power law was used to identify wavenumber ranges (about 1.5 decades) associated with inactive eddy motion. The measured T'_s wavelet spectra and $u'T'_s$ cospectra identified with this wavenumber range demonstrate that much of the T'_s energy and $\langle u'T'_s \rangle$ are due to inactive eddy motion, where the angle brackets indicate time averaging. Hence, in contrast to the laboratory experiments of *Owen and Thomson* [1963], it is argued that skin temperature perturbations at the canopy-atmosphere interface of a grass-covered surface (small thermal inertia) are strongly dependent on the inactive eddy motion produced in the outer layer of the ABL.

1. Introduction

The estimation of sensible heat flux (H) from remotely sensed skin foliage temperature (T_s) in conjunction with resistance analog or similarity formulations has received much attention recently [see, e.g., *Kaneko and Hino*, 1996; *Brutsaert and Sugita*, 1996; *Sugita and Brutsaert*, 1996, 1992; *Qualls and Brutsaert*, 1996; *Brutsaert et al.*, 1993]. For example, *Monin and Obukhov* [1954] similarity theory (MOST) can be used to estimate H from T_s if the friction velocity (u_*), the heat roughness length (z_{oh}), and the Obukhov length (L) are known using

$$\langle T_s \rangle - \langle T_a(z) \rangle = \frac{\langle w'T' \rangle}{ku_*} \left[\ln \left(\frac{z}{z_{oh}} \right) - \Psi_h \left(\frac{z}{L} \right) \right] \quad (1)$$

where Ψ_h is the atmospheric stability correction function for heat [see *Brutsaert*, 1982; *Kader and Yaglom*, 1990; *Katul and Parlange*, 1992], $T_a(z)$ is the air temperature at height z above the zero-plane displacement, w' and T' are the turbulent vertical velocity and temperature fluctuations, respectively ($\langle w' \rangle = \langle T' \rangle = 0$), and the angle brackets indicate time averaging over sampling period T_p (~20–30 min).

¹School of the Environment, Duke University, Durham, North Carolina.

²Center for Hydrologic Science, Duke University, Durham, North Carolina.

³Jet Propulsion Laboratory, California Institute of Technology, Pasadena.

⁴Institute of Statistics and Decision Sciences, Duke University, Durham, North Carolina.

Copyright 1998 by the American Geophysical Union.

Paper number 98WR00293.
0043-1397/98/98WR-00293\$09.00

Advancement in remote sensing measurement techniques permits the rapid estimation of T_s over large areas at nearly one time instant (nadir speed of a Sun synchronous satellite at 700 km is about 6 km s⁻¹ as in the work by *Chen* [1985]). Hence, in a first-order analysis, it is assumed that remotely sensed T_s represents $\langle T_s \rangle$ permitting the use of (1) in estimating H .

Departure of $\langle T_s \rangle$ from T_s for a dense canopy is dependent, among other things, on the turbulent velocity (u'_i) statistics, where $u'_1(=u')$, $u'_2(=v')$, $u'_3(=w')$ are the turbulent velocity components along $x_1(=x)$, $x_2(=y)$, and $x_3(=z)$, and x_1 , x_2 , and x_3 are the longitudinal, lateral, and vertical Cartesian coordinates, respectively, with x_1 aligned along the mean horizontal wind direction (both index and meteorological notations are used interchangeably), and primes denote fluctuations from a time-averaged quantity. The dependence of T'_s on velocity has been well documented in laboratory and some field experiments; however, the structural properties of eddy motion responsible for the production of T'_s and $\langle u'_1 T'_s \rangle$ is much less understood when compared to $\langle u'_3 T'_a \rangle$ (or sensible heat) and is the subject of the present investigation.

Early experiments by *Owen and Thomson* [1963] on heat transfer between a roughened surface and a stream of incompressible turbulent fluid flow demonstrated that horseshoe eddies scour the surface thereby transporting heat from the surface and the more vigorous turbulent flow in the neighborhood of the roughness crest. Scouring and eddy penetration result in rapid cooling of skin temperature producing large excursions in T_a . Such laboratory experiments were conducted above bluff-rough elements and may not well represent permeable-rough elements [e.g., *Chamberlain*, 1966; *Brutsaert*, 1979; *Bache*, 1986; *Massman*, 1987]. Measurements within forested

systems conclude that eddies of the order of the canopy height (h) are responsible for much of the sensible heat transport (see *Raupach et al.* [1996] for a review). Whether h is also the predominant length scale for turbulent statistics such as $\langle u'_i T'_s \rangle$ has not been rigorously investigated.

For permeable-rough surfaces such as grass, additional complications arise due to waving of roughness elements as discussed by *Finnigan* [1979]. This complication was observed using infrared surface temperature (IRT) measurements above a grass site by *Vining and Blad* [1992]. They found that high wind speeds were responsible for producing a planophile canopy in which the leaves were more horizontally oriented owing to bending of the grass leaves. Both waving canopy motion and eddy-scouring activity are governed by turbulent velocity statistics (e.g., gusts). Understanding the phenomenological relationship between turbulent velocity and skin temperature perturbations motivated the present study.

The objective of the present study is to investigate the temporal variability in surface temperature induced by surface layer turbulent velocity. Specifically, spectral and cospectral properties of u' , T'_a , and T'_s are measured and discussed in order to identify characteristic length scales of eddy motions responsible for such interactions. High-frequency infrared temperature along with atmospheric surface layer (ASL) air temperature and velocity were measured and analyzed over a grass-covered forest clearing at the Duke Forest near Durham, North Carolina.

2. Methods of Analysis

Much of the u' interactions with T'_s are due to localized eddy motion in the time domain (e.g., gusts), and hence a localized basis function in the time domain is preferred for spectral and cospectral analysis vis-a-vis a nonlocal Fourier basis. A localized basis function in the time domain has some advantages over its Fourier counterpart due to its ability to concentrate much of the turbulent energy in few wavelet coefficients [*Katul and Vidakovic*, 1996] and capture both the energy disbalance in the frequency domain and the intermittency in the time domain. In addition, wavelet spectra are better suited than their Fourier counterpart for investigating power laws at low wavenumbers since no data conditioning (i.e., arbitrary tapering and windowing) is required. Data conditioning significantly distorts the spectrum estimation at low wavenumbers [*Kaimal and Finnigan*, 1994], and such distortions are not advantageous for analyzing inactive eddy signatures. For completeness, key derivations of wavelet spectra and cospectra calculations are first reviewed.

2.1. Wavelet Analysis

Orthonormal wavelet transforms are used since the basis functions are orthogonal and mutual independence of wavelet coefficients is guaranteed. As shown by *Daubechies* [1992], using a logarithmic uniform spacing for the scale discretization with increasingly coarser spatial resolution at larger scales, a complete orthogonal wavelet basis can be constructed that allows the decomposition of any measured turbulent flow variable (e.g., u' , w' , T'_a , and T'_s) vector $f(x_j)$ into N wavelet coefficients (where $j = 0, 1, \dots, N - 1$) and $\langle f(x_j) \rangle = 0$. Unlike Fourier transforms, many wavelet basis functions are available for this decomposition.

2.2. Fast Wavelet Transform (FWT)

The Haar wavelet basis is selected for its differencing characteristics and its locality in the time domain. Furthermore, the Haar wavelet has only two taps and does not introduce any edge effects in the transformed series. The Haar basis $\psi_{a,b}(x) = (a^{-1/2})\psi((x - b)/a)$, where $a = 2^m$ and $b = 2^m i$ for $i, m \in \mathbf{Z}$, is given by

$$\Psi(x) = \begin{cases} 1 & 0 < x < 1/2 \\ -1 & 1/2 \leq x < 1 \\ 0 & \text{elsewhere,} \end{cases} \quad (2)$$

where i and m are position and scale indices, respectively. For the Haar basis function the wavelet coefficients $C^{(m+1)}(k)$ and the coarse-grained signal $S^{(m+1)}(k)$ (i.e., a low-pass-filtered series) at scale $m + 1$ can be determined from the signal $S^{(m)}$ at scale m using

$$C^{(m+1)}(i) = \frac{1}{\sqrt{2}} [S^{(m)}(2i - 1) - S^{(m)}(2i)] \quad (3)$$

$$S^{(m+1)}(k) = \frac{1}{\sqrt{2}} [S^{(m)}(2i - 1) + S^{(m)}(2i)] \quad (4)$$

for $m = 0$ to $M - 1$, $i = 0$ to $2^{M-m-1} - 1$, and $M = \log_2(N)$, N is the number of samples (integer power of 2). The coarse-grained signal is a low-pass-filtered function obtained by simple block averaging (see *Daubechies* [1992] for other types of filters). The wavelet coefficients (C) and coarse-grained signal (S) are calculated from simultaneous application of (3) and (4) to the measurement vector (stored in $S^{(0)}$) for $m = 0$ to $M - 1$, where $\langle S^{(0)} \rangle = 0$. Such algorithm yields $N - 1$ wavelet coefficients defining the orthonormal Haar wavelet transform of the measured flow variable $S^{(0)}$ [see, e.g., *Katul et al.*, 1994; *Katul and Parlange*, 1994; *Katul and Vidakovic*, 1996]. The above pyramidal procedure, known as fast wavelet transforms (FWT), requires of the order of N computations vis-a-vis the $N \log_2 N$ for fast Fourier transforms (FFT).

2.3. Wavelet Spectra and Cospectra

The $N - 1$ discrete Haar wavelet coefficients also satisfy the energy conservation:

$$\sum_{j=0}^{j=N-1} f(j)^2 = \sum_{m=1}^{m=M} \sum_{i=0}^{i=(2^{M-m}-1)} [C^{(m)}(i)]^2. \quad (5)$$

which is analogous to Parseval's identity in Fourier series. The total energy T_E contained in a scale $R_m (= 2^m dy)$ can be computed from the sum of the squared wavelet coefficients at scale index (m) using

$$T_E(R_m) = \frac{1}{N} \sum_{i=0}^{i=(2^{M-m}-1)} (C^{(m)}[i])^2; \quad (6)$$

where

$$\langle S^{(0)2} \rangle = \sum_{m=1}^{m=M} T_E(R_m)$$

where $dy = f_s^{-1} \langle U \rangle$, typically estimated using *Taylor's* [1938] hypothesis, is the measurement spacing in physical space, and f_s is the sampling frequency (5 Hz for this experiment). From this identity, it is possible to derive the Haar wavelet power

spectrum (energy per unit wavenumber) for a given angular wavenumber K_m corresponding to scale R_m as

$$K_m = 2\pi/R_m. \quad (7)$$

The wavenumber definition in (7) was first proposed by *Meneveau* [1991a, b] and is widely used in turbulence research [Katul and Parlange, 1994; Yamada and Ohkitani, 1990; 1991a, b; Hayashi, 1994; Katul and Vidakovic, 1996]; however, such K_m definition is not unique [Kumar and Foufoula-Georgiou, 1994; Farge, 1992]. Hence the power spectral density function $E(K_m)$ is computed by dividing T_E by the change in wavenumber $\Delta K_m (= 2\pi 2^{-m} dy^{-1} \ln[2])$ so that

$$E(K_m) = \frac{\langle\langle (C^{(m)}[i])^2 \rangle\rangle dy}{2\pi \ln(2) 2^{-m}} \quad (8)$$

where double angle brackets indicate averaging over all values of (i) at scale index (m) (see *Szilgayi et al.* [1996] for discussion on alternative definition of ΔK_m). Notice that the wavelet power spectrum at wavenumber K_m is directly proportional to the average of the squared wavelet coefficients at that scale. Because the power at K_m is determined by averaging many squared wavelet coefficients, the wavelet power spectrum is generally smoother than its Fourier counterpart.

The Haar wavelet cospectrum of two turbulent flow variables (e.g., u' and T'_s) can be calculated from their respective wavelet coefficient vectors ($C_U^{(m)}$ and $C_{T_s}^{(m)}$) at wavenumber K_m using

$$E_{U,T_s}(K_m) = \frac{\langle\langle (C_U^{(m)}[i])(C_{T_s}^{(m)}[i]) \rangle\rangle dy}{2\pi 2^{-m} \ln(2)} \quad (9)$$

where $\langle u' \rangle = \langle T'_s \rangle = 0$, and

$$\langle u' T'_s \rangle = \frac{1}{N} \sum_{m=1}^{m=M} \sum_{i=0}^{i=(2^m-1)} [C_U^{(m)}(i) C_{T_s}^{(m)}(i)] \quad (10)$$

as discussed by *Hayashi* [1994], *Katul and Parlange* [1994, 1995], and *Katul et al.* [1996a]. Both wavelet spectra of T'_s , T'_a , and u' and the cospectra between u' and T'_s and u' and T'_a are used to identify the primary scales responsible for much of the $\langle T_s'^2 \rangle$ and $\langle u' T'_s \rangle$ production.

3. Experiment

The experiment was conducted from September 18 to September 21, 1996, at the Blackwood Division of the Duke Forest near Durham, North Carolina. The site elevation, latitude, and longitude are 163 m, 35°98'N, and 79°8'W, respectively.

3.1. Site Description

The site, a dense grass-covered forest clearing, is 480 m long (north-south direction) and 305 m wide (east-west direction). The clearing is surrounded by a uniform 10–13 m tall Loblolly pine forest and is covered with *Alta Fescue* grass. Earlier in the month, hurricane Fran swept through the region and saturated much of the soil. During the experiment, the mean grass height (h) measured at the center of the clearing was 1 m. The western and northern edges of the clearing are bounded by two unpaved roads.

3.2. Instruments

The instruments were positioned on a central mast, located 200 m from the northern edge. Instrumentation for this exper-

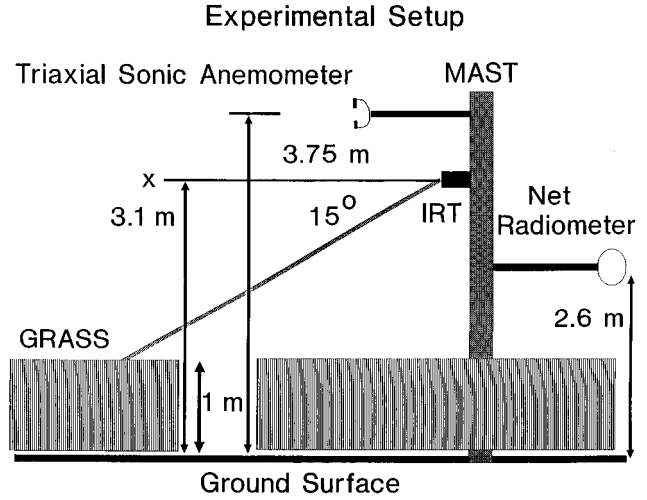


Figure 1. Schematic of instrumentation heights during the experiment.

iment consisted of a three-axis Gill anemometer, REBS (Q7) Net Radiometer, and an Everest Infrared Thermometer (IRT). Descriptions of the three-axis Gill anemometer are given by *Szilgayi et al.* [1996] and *Katul et al.* [1995]. The Gill sonic anemometer was positioned at 3.75 m in the ASL above the ground surface ($>3.5 h$), while the net radiometer was positioned at 2.6 m above the ground surface and 1.3 m away from the mast. The IRT was mounted, facing north, at a height of 3.1 m and angled 15° from vertical (75° from horizontal with a 15° field of view) producing a ground footprint of approximately 16 m. At $z = h$, the footprint is 11 m long, 2 m wide with a centroid 8 m out from the mast. This view angle biases the IRT measurements toward the upper third of the grass canopy for which much of the heat exchange with the atmosphere occurs (see Figure 1). Given the dense and well-watered state of the grass during the experiment, such angular effects are considered minor for the analysis of rapid excursions in T_s . We also note that angular effects on mean skin temperature was reported minor for well water agricultural crops as by *Fuchs* [1990], the alfalfa measurements of *Lagouarde and Kerr* [1993], and the short-crop wheat experiment of *Huband and Monteith* [1986]. In the appendix, the angular effects on the high-frequency measurements are explored in greater details from a separate experiment performed in October 1997 over a drier soil moisture state for the same grass field. Dry moisture content state tends to amplify angular dependencies in IRT measurements. We found that angular effects can be significant for the mean surface temperatures (primarily due to heat source area differences) but are minor for analyzing mechanisms responsible for the generation of skin temperature perturbations.

3.3. Measurements

The IRT and sonic anemometer velocity were sampled at 5 Hz using a 21X Campbell Scientific Micrologger. The measurements were transferred from the logger to a portable computer via an optically isolated RS232 interface and stored on the hard drive for future processing. The raw measurements were fragmented into individual runs, with each run duration being 27.3 min, so that $N = 2^{13}$ measurements per flow variable per run. A sample run is shown in Figure 2. In Figure 2 a typical grass surface emissivity of 0.95 [see *Brutsaert*, 1982]

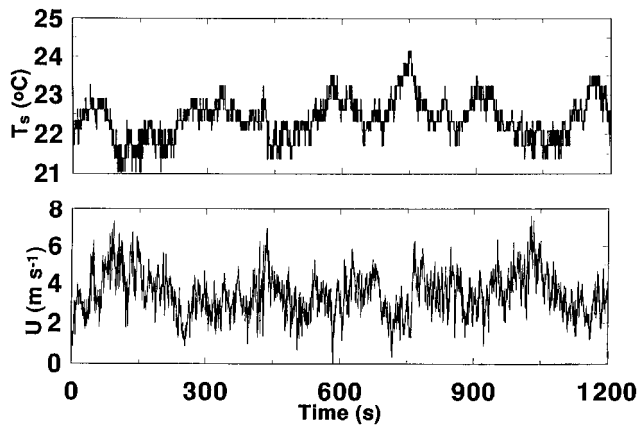


Figure 2. (top) A sample IRT measured T_s and (bottom) sonic anemometer measured U_1 during the 3-day experiment. For display purposes of kinetic temperature, the assumed grass emissivity is 0.95 as in the work by *Brutsaert* [1982]. The correlation coefficient between u' and T_s' is -0.38 for this run but varied from -0.05 to -0.63 throughout the experiment.

is used to convert radiometric to skin temperatures. Notice that T_s can change by 2.5°C in about 100 s depending on the variability in longitudinal velocity. For this sample run the correlation coefficient between u' and T_s' is -0.38 though values ranging from -0.05 to -0.63 were measured in this study. For 23 runs the squared correlation coefficient between u' and T_s' exceeded the squared correlation coefficient between u' and T_a' measured by the sonic anemometer. Such large absolute correlation coefficients between T_s (measured from an 11 m by 2 m source area with a centroid 8 m away from the tower) and velocity perturbations can only be explained by eddy motions significantly contributing to both u' and T_s' when compared to the T_a' signal.

The net radiation along with mean air temperature and relative humidity were sampled every 1 s and averaged over the sampling period. Runs were excluded if cloudy sky conditions prevailed, trends in the air temperature time series were noted, or sensible heat flux did not exceed 20 W m^{-2} (to avoid transition periods). The experiment resulted in 37 runs satisfying the above three criteria.

4. Results

In the results and discussion, power laws and eddy sizes responsible for much of the velocity, air, and surface temperature variances are identified via wavelet analysis. Then the phenomenology of eddy motion responsible for the interaction between T_s' and u' is analyzed from cospectral measurements. In the context of *Townsend's* [1976] hypothesis the characteristic eddy sizes responsible for the interaction between T_s' and u' are inactive eddies with length scale as large as the atmospheric boundary layer height. In contrast to *Townsend's* inactive eddy motion hypothesis, direct extension of the horseshoe eddy model of *Owen and Thomson* [1963] predicts a characteristic length scale comparable to the canopy height. Hence the proposed wavelet analysis below will permit us to discern which type of eddy motion is responsible for skin temperature perturbations and their interaction with the turbulent velocity.

4.1. Townsend's [1976] Hypothesis

Townsend [1976] proposed that turbulent motion in the inner region of a neutral boundary layer can be decomposed into an active part, which produces the shear stress $\langle u'w' \rangle$ and whose statistical properties are universal functions of u_* and z , an inactive part, and a fine scale part which follows the classical *Kolmogorov* [1941] theory. Origins of inactive motion are partly due to pressure fluctuations and partly due to large-scale vorticity in the outer layer [*Bradshaw*, 1967; *Antonia and Raupach*, 1993]. Furthermore, it is noted that while inactive eddy motion contributes to the shear stress in the outer layer, it does not contribute to $\langle u'w' \rangle$ in the inner (or surface) layer. A direct consequence of such a decomposition is that inactive eddy motion should be confined to the low wavenumber parts of the u' spectrum in the inner region. Direct testing of *Townsend's* hypothesis was undertaken by *Perry et al.* [1986], who demonstrated that inactive eddy motion scales with boundary layer height and u_* . Since the analysis considers T_s' rather than kinetic temperature, surface emissivity corrections are not considered.

4.2. Wavelet Spectral Analysis

The Haar wavelet spectra (energy per unit wavenumber) for u' and T_s' are computed for all 37 runs using (8) and shown in Figures 3a and 3b. The one-dimensional wavenumber is computed using *Taylor's* [1938] hypothesis and the sonic anemometer velocity measurements. It should be noted that *Taylor's* hypothesis may not precisely convert the time to wavenumber domain due to differences between the true convection velocity and $\langle U \rangle$ [see, e.g., *Fisher and Davies*, 1964; *Lumley*, 1965]. Nonetheless, for order of magnitude scale estimation and power law investigations, such an approximation appears reasonable as evidenced by the two-point ASL measurements of *Powell and Elderkin* [1974] and *Mizuno and Panofsky* [1975]. For the u' spectrum, the -1 and $-5/3$ power laws, associated with the inactive [*Townsend*, 1976; *Bradshaw*, 1967] and inertial eddy motions, respectively, are also shown in Figure 3a.

4.2.1. Identification of the inactive eddy motion wavenumber range from the velocity spectrum. As earlier stated, the decomposition into an active component which is dependent

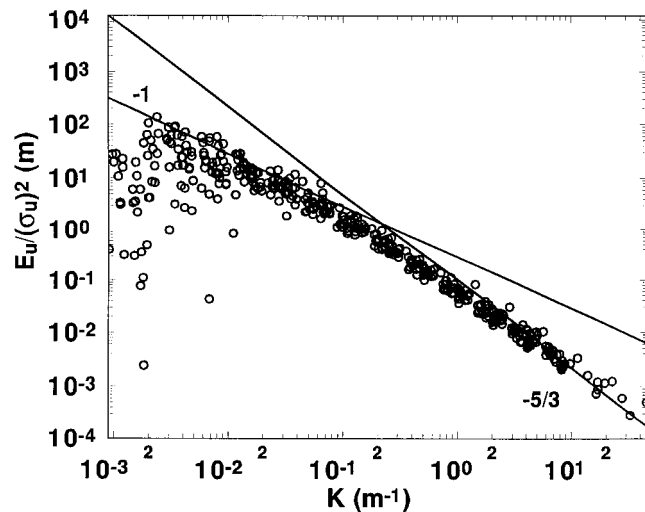


Figure 3a. Normalized Haar wavelet power spectra for u' (E_u/σ_u^2) as a function of wavenumber (K) for all runs, where $\sigma_u^2 = \langle u'^2 \rangle$. The -1 and $-5/3$ power laws are also shown.

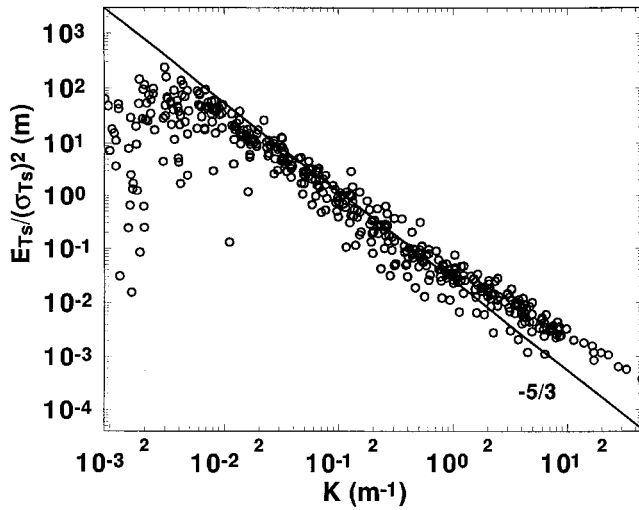


Figure 3b. Same as Figure 3a, but for T'_s . The $-5/3$ power law is shown.

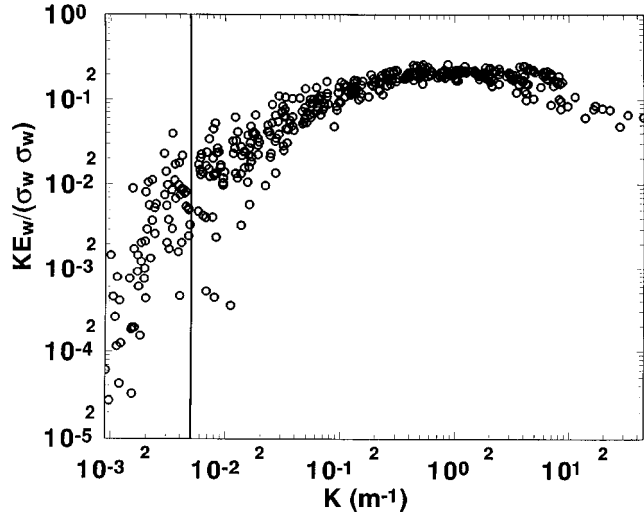


Figure 4b. Same as Figure 4a, but for vertical velocity (KE_w).

on u_* and z , and an inactive component which is produced by turbulence in the outer region of the ABL, has received much attention recently (see Raupach et al., 1991; Hogstrom, 1990 for reviews) yet no clear “signature” mechanism has been proposed by these authors. Using simultaneous static pressure and longitudinal velocity measurements in the ASL at the same grass clearing, Katul et al. (1996b) demonstrated that signatures of inactive eddy motion is a -1 power-law in the longitudinal velocity spectrum (see also Kader and Yaglom, 1991). We used the -1 power-law spectral signature to identify inactive eddy motion for this data set and found that the approximate inactive eddy motion wavenumber range is between $K = 0.003 \text{ m}^{-1}$ to 0.1 m^{-1} .

4.2.2. Evidence of inactive eddy motion from wavelet spectra. The T'_s spectra follow an extensive $-5/3$ power law for $K = 0.005 \text{ m}^{-1}$ to 0.5 m^{-1} as evidenced in Figure 3b and much of this wavenumber range overlaps the inactive eddy motion wavenumber range in Figure 3a. For scales much larger

than z (in the following discussion, much larger implies at least an order of magnitude larger), the σ_u energy is mainly associated with the inactive eddy motion as evidenced in Figure 4a, in agreement with Yaglom’s [1994] recent dimensional analysis, the measurements of Panofsky and Dutton [1984], and the theoretical arguments of Katul et al. [1996b]. To further verify that such low wavenumber eddy motion identified in Figures 3a and 4a is associated with the inactive eddy motion, the total energy spectrum of the vertical velocity is computed and shown in Figure 4b. Notice in Figure 4b that much of the σ_w energy is associated with wavenumbers comparable to z (i.e., $K \sim 1.5 \text{ m}^{-1}$) as expected from Monin and Obukhov surface layer similarity; hence the energy contribution from inactive eddy motion on W is small ($<5\%$). Interestingly, the measurements in Figure 4c suggest that much of σ_{T_s} is also associated with the inactive eddy motion identified by the -1 power law of Figure 3a. The flat portion at large wavenumbers of the total T'_s energy spectrum (Figure 4c) is partly due to instrumentation noise and the 1 s shutter speed of the Everest IRT.

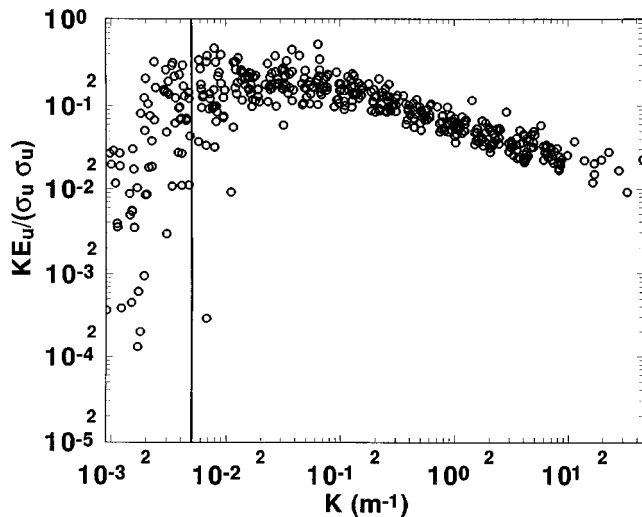


Figure 4a. Total wavelet energy (KE_u) as a function of wavenumber (K) for all runs. The vertical solid line is for a scale of 1200 m.

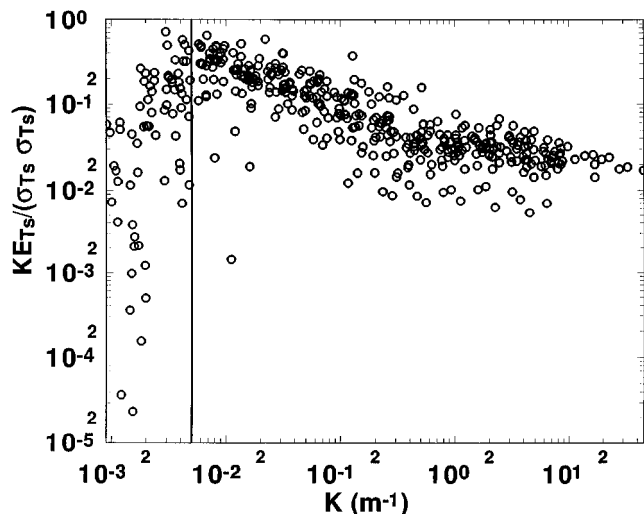


Figure 4c. Same as Figure 4a, but for T'_s (KE_{T_s}).

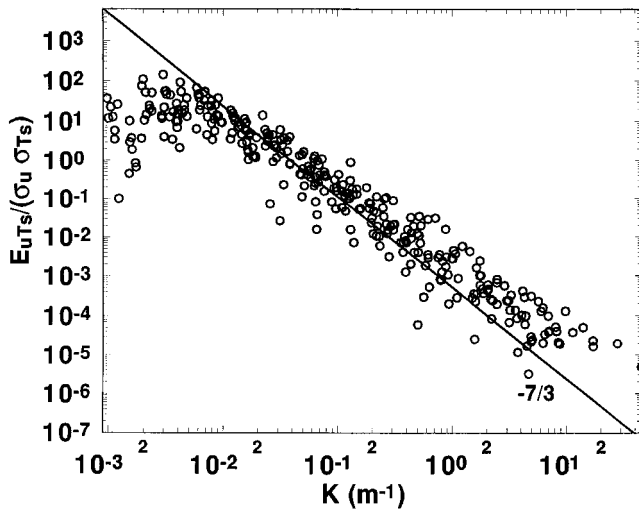


Figure 5a. Normalized Haar wavelet cospectra between longitudinal velocity and skin temperature (E_{uT_s}) as a function of wavenumber. The ordinate axis is multiplied by -1 to permit a log scale. The $-7/3$ power law is shown.

4.3. Wavelet Cospectral Analysis

From section 4.2 it is evident that the inactive eddy motion significantly contributes to σ_{T_s} and σ_u . To investigate whether this eddy motion is also responsible for the interaction between the u' and T'_s perturbations, Haar wavelet cospectra are computed using (9) for all 37 runs and shown in Figure 5a. Notice in Figure 5a that E_{uT_s} cospectrum decays rapidly ($K^{-1.96}$) suggesting rapid decoupling between turbulent velocity and skin temperature perturbations with increasing wavenumber. Since atmospheric reflected radiation, which is a function of T'_a , contributes to the IRT measured longwave radiation [Huband and Monteith, 1986; Kohsiek et al., 1993; Feijt and Kohsiek, 1995; Mathur et al., 1996], it is possible that much of the T'_s variability and the interaction between u' and T'_s are due to T'_a . For this purpose, the E_{uT_a} cospectrum as well as the T'_a spectrum are computed for all runs and displayed in Figures 5b and 5c, respectively. Notice the clear co-spectral (Figures 5a

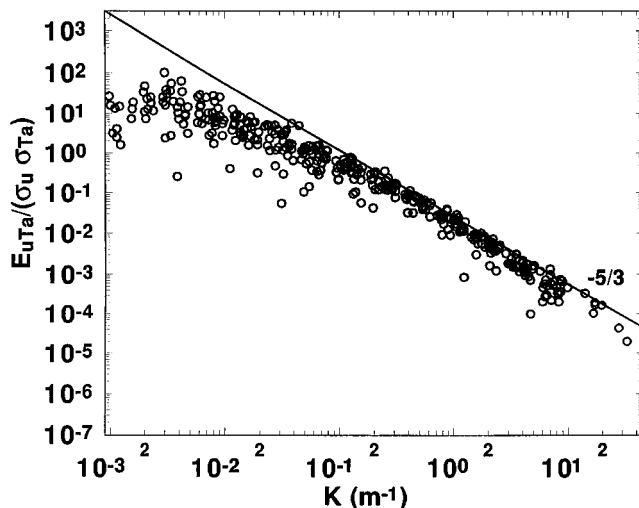


Figure 5b. Same as Figure 5a, but for longitudinal velocity and air temperature (E_{uT_a}).

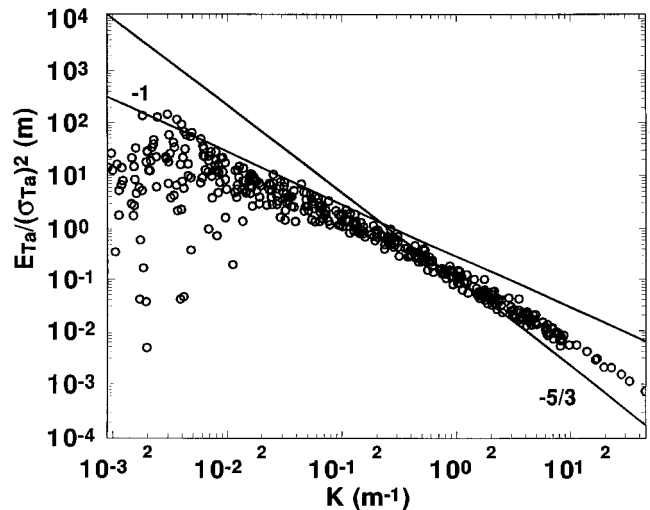


Figure 5c. Same as Figure 3a, but for T'_a .

and 5b) and spectral (Figures 3b and 5c) dissimilarities between T'_s and T'_a implying that interaction between u' and T'_s cannot be explained by locally reflected longwave radiation contribution to the IRT measurements just above the heat source area. In fact, the wavelet cospectral decomposition of $\langle u'T'_s \rangle$ in Figure 6 attributes much of the surface cooling to eddies comparable to the ABL height scale. This $u'T'_s$ interaction peaks at a scale (solid vertical line) of about 1200 m and is comparable to estimates of the mean neutral ABL height [Tennekes, 1973]. The decorrelation between $u'T'_s$ is much more rapid ($K^{-1.96}$) when compared to $u'T'_a$ ($K^{-5/3}$) suggesting that fine-scale turbulence in the ASL contributes little to skin temperature perturbations.

5. Conclusions

This study demonstrated the following:

1. For cloud free conditions the turbulent velocity can induce large skin temperature perturbations ($>2^\circ\text{C}$) within short time intervals (<1 min). It is shown using wavelet cospectra that such velocity-skin temperature interaction occurs at scales comparable to the ABL height and is associated with inactive eddy motion. Our finding is inconsistent with the dimensional arguments of Owen and Thomson [1963] or Yaglom and Kader [1974], who proposed that all statistical properties of turbulence within roughness elements scale with u_* and h . Owen and Thomson [1963] argued that horseshoe eddy motion with a characteristic length scale comparable to the roughness height (in their experiment sand-roughened surface), scours the surface thereby removing heat (see also Yaglom and Kader [1974] for different argument leading to the same characteristic length scale for pipe flow). While this argument was validated for $\langle w'T'_a \rangle$ by many field experiment [Raupach et al., 1996], it clearly fails to model the statistical properties of $\langle u'T'_s \rangle$. Our analysis suggests that inactive eddy motion, comparable to the ABL height, is mainly responsible for $\langle u'T'_s \rangle$.

2. Much of the surface layer velocity and skin temperature variance (σ_u^2 and $\sigma_{T_s}^2$) is due to inactive eddy motion. The inactive eddy motion significantly contributes to σ_u but not to $\langle u'w' \rangle$ or σ_w as evidenced by our measurements and many other ASL and laboratory experiments. We note that wind tunnel studies by Raupach [1981] suggest that the statistical

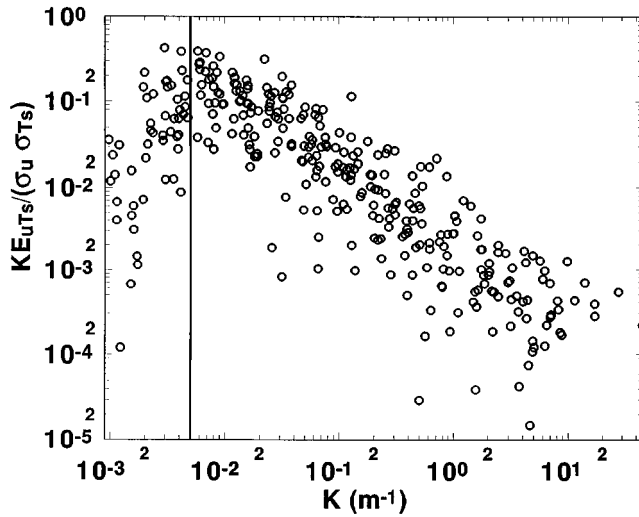


Figure 6. Total normalized Haar wavelet covariance between u' and T'_s ($KE_{uT'_s}$) as a function of wavenumber K . The ordinate axis is multiplied by -1 to permit a log scale. The vertical solid line is for a scale of 1200 m and is the maximum scale at which u' and T'_s interact.

properties of inactive eddy motion in the ASL are insensitive to surface roughness. Whether the same generalization can be made for field conditions remains to be tested given the thermal inhomogeneity of natural surfaces and the enhancement of heat transport due to canopy waving motion.

3. For inactive eddy motion, our measurements revealed that the spectral and cospectral power laws for E_{T_s} and E_{uT_s} are $-5/3$ and -1.96 , respectively. The rapid decay in the E_{uT_s} cospectrum suggests rapid decoupling between the surface layer velocity field and skin temperature perturbations with increasing wavenumber. It is also demonstrated that both spectral and co-spectral power laws in E_{T_s} and E_{uT_s} contrast the measured E_{T_a} and E_{uT_a} for the inactive eddy motion wavenumber range.

Appendix: Effects of View Angle on Skin Temperature Statistics

In this appendix, the effects of view angle on the statistics of T_s are examined from a separate experiment performed at the same grass-covered clearing from October 7 till October 11, 1997 (DOY 280–284). Two infrared thermometers, one positioned at 45° and the other at 75° from the horizontal (i.e., same as the 1996 experiment), were situated at 3.1 m above the ground surface. Both IRTs are sensing nonoverlapping heat source areas of different sizes (yet large enough to aggregate sufficient foliage). The Q7 net radiometer was positioned at

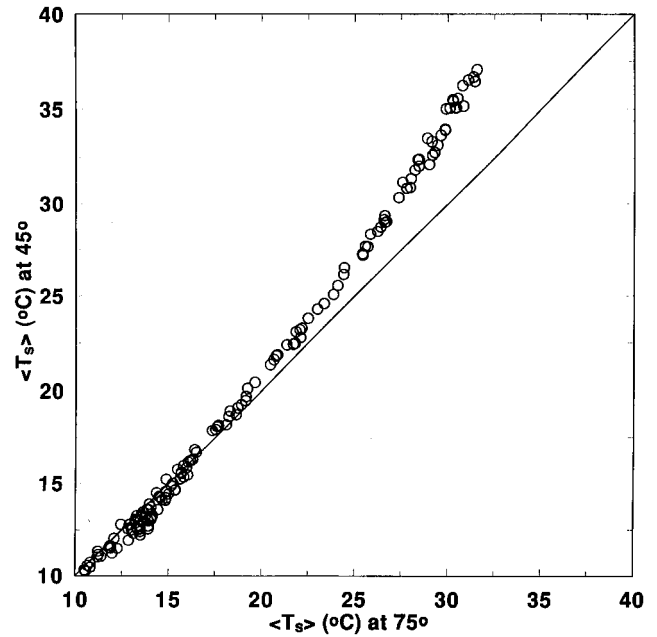


Figure A1. Comparison between $\langle T_s \rangle$ measured at view angles 45° and 75° (emissivity set to unity) for all 152 runs. The 1:1 line is also shown.

the same height as the 1996 experiment. The sampling frequency, duration, and logging method were identical to the 1996 experiment. The experiment resulted in 152 runs (night and day included here). The soil moisture conditions in the top 10 cm were much drier ($0.1 \text{ cm}^3 \text{ cm}^{-3}$) when compared to the 1996 experiment ($0.36 \text{ cm}^3 \text{ cm}^{-3}$). Hence any angular dependence should be amplified for such dry soil moisture conditions. The experiment was designed to test whether perturbations about the mean surface temperature sensed from one heat source area are similar to another nonoverlapping heat source area of different dimensions sensed by an IRT at a different angle. The comparison between the two IRT sensors is discussed next.

A.1. Angular Effects on the Mean Skin Temperature

From Figure A1 and Table A1 it is apparent that the two IRTs have different mean values (especially for warmer daytime surface conditions). This difference is expected since the two source areas are not identical.

A.2. Angular Effects on the Fluctuating Skin Temperature

From Figure A2 and Table A1 the two standard deviations are not identical though they are strongly correlated ($R^2 = 0.94$). Note that if the view angle is the primary mechanism

Table A1. Effects of View Angle on IRT Measured Statistics

Comparison	$\langle T_{45} \rangle = A \langle T_{75} \rangle + B$	$\sigma_{45} = A \sigma_{75} + B$
Slope (A)	1.27	1.28
Intercept (B)	-4.24	0.002
Coefficient of determination (R^2)	0.995	0.941
Standard error of estimate (SEE), $^\circ\text{C}$	0.61	0.12

The regression comparisons are also shown, where $\langle T_{45} \rangle$ and $\langle T_{75} \rangle$ are the mean IRT measured brightness temperatures at view angles 45° and 75° , and σ_{45} and σ_{75} are the standard deviations about the means.

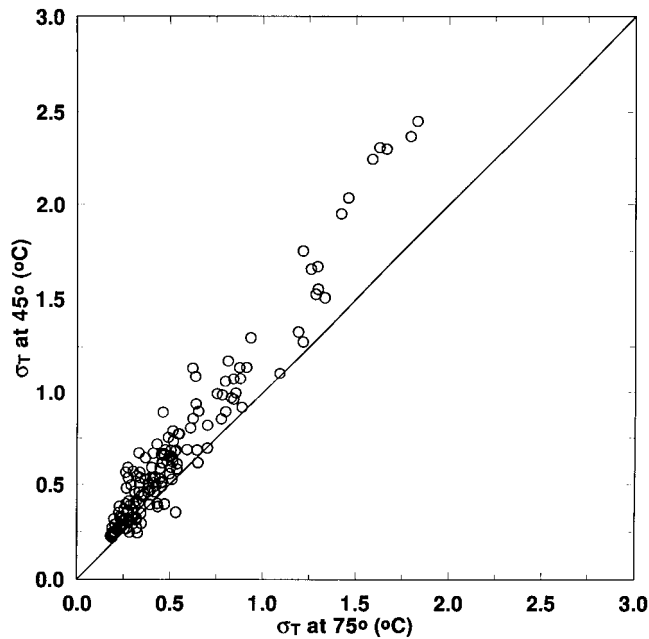


Figure A2. Comparison between $\langle T_s'^2 \rangle^{1/2}$ for the same runs as Figure A1.

responsible for departures from the 1:1 relationship in Figure A1, then it is expected that the IRT positioned at 45° result in lower variances than the IRT positioned at 75° since the latter biases measurements toward the upper part of the foliage (which is better coupled to the air stream aloft). The measurements in Figure A2 and regression analysis in Table A1 demonstrate an opposite trend. In fact, the variance slope differences in Table A1 ($=1.28$) are comparable to the mean IRT slope differences ($=1.27$). Such differences in source areas are responsible for the departure from the variance 1:1 line.

That the two variances are strongly correlated ($R^2 = 0.94$) suggests that the same mechanisms are influencing both IRT sensor measurements. This hypothesis was tested in Figure A3, which displays the 30-min correlation coefficients between the

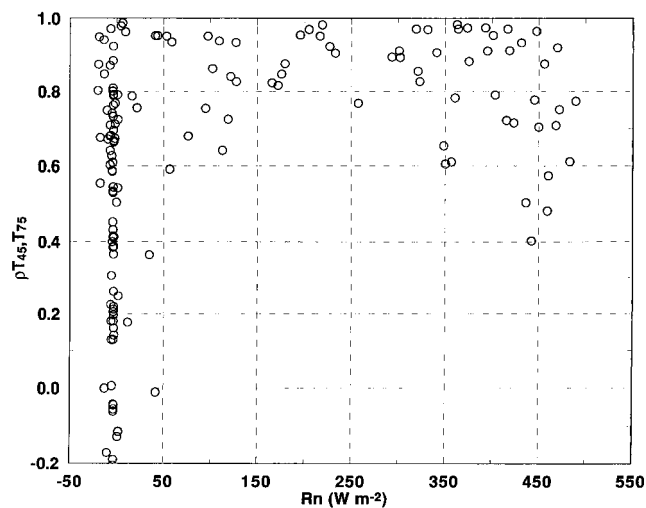


Figure A3. The variation of the correlation coefficient between the two IRT measurements with R_n for all runs in Figure A1.

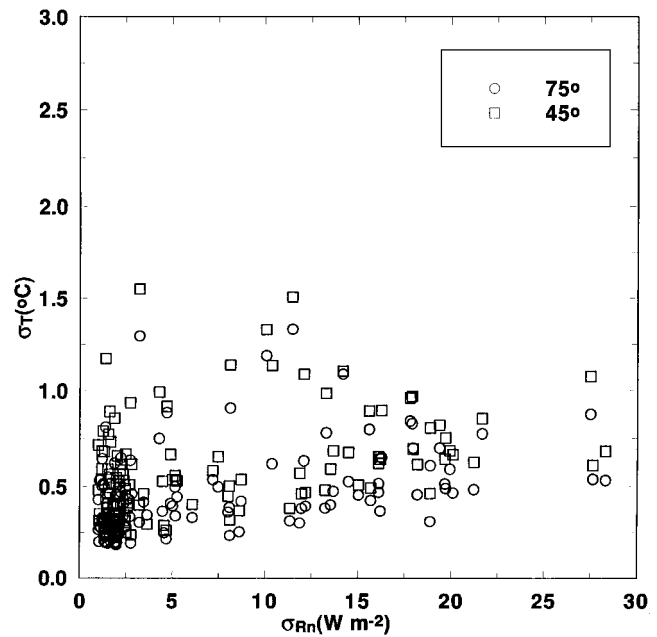


Figure A4. The variation of σ_T with σ_{Rn} for all runs in Figure A1 (with the exception of seven points for which spikes were detected in net radiation time series).

two IRTs as a function of R_n . Notice that when R_n exceeds 50 W m^{-2} , the correlation coefficient between the two IRTs vary between 0.6 and 0.99 with the majority of runs ($=43$) having a correlation coefficient exceeding 0.8. It is possible that variability in R_n within a 30-min time interval produces such strong correlation coefficients between the two IRT signals (energy vis-a-vis a turbulence generated mechanism). We tested this hypothesis in Figure A4 and found no clear relationship between the standard deviations in R_n and T_s for both view angles. Therefore we conclude from this experiment that while angular effects significantly affect the mean surface temperature for dry soil conditions, they are minor for the analysis of mechanisms producing T_s perturbations. Such a conclusion stems from the fact that both IRT readings at different view angles are strongly correlated.

Acknowledgments. The authors would like to thank Judd Edeburn and the Duke Forest staff for their help at the Blackwood Division of the Duke Forest, Greg Kuhn and Chunta Lai for assisting in the field setup, Ned Patton for his helpful comments, and John Albertson for lending us another IRT sensor to perform the October 1997 experiment described in the appendix. This project was funded, in part, by the U.S. Department of Energy's (DOE) National Institute of Global Environmental Change (NIGEC) through NIGEC's Southeast Regional Center at the University of Alabama, Tuscaloosa, under cooperative agreement DEFC03-90-ER61010, the Science Division of Jet Propulsion Laboratory, and the National Science Foundation Grants DMS-9626159 and BIR-9512333.

References

- Antonia, R. A., and M. R. Raupach, Spectral scaling in a high Reynolds number laboratory boundary layer, *Boundary Layer Meteorol.*, 65, 289–306, 1993.
- Bache, D. H., On the theory of gaseous transport to plant canopies, *Atmos. Environ.*, 20, 1379–1388, 1986.
- Bradshaw, P., Inactive eddy motion and pressure fluctuations in turbulent boundary layers, *J. Fluid Mech.*, 30, 241–258, 1967.
- Brutsaert, W., Heat and mass transfer to and from surfaces with dense

- vegetation or similar permeable roughness, *Boundary Layer Meteorol.*, 16, 365–388, 1979.
- Brutsaert, W., *Evaporation into the Atmosphere: Theory, History, and Applications*, 300 pp., Kluwer Acad., Norwell, Mass., 1982.
- Brutsaert, W., and M. Sugita, Regional surface fluxes from satellite-derived surface temperature (AVHRR) and radiosonde profiles, *Boundary Layer Meteorol.*, 58, 355–366, 1992.
- Brutasert, W., and M. Sugita, Sensible heat transfer parameterization for surfaces with anisothermal dense vegetation, *J. Atmos. Sci.*, 53, 209–216, 1996.
- Brutsaert, W., A. Hsu, and T. J. Schumge, Parameterization of surface heat fluxes above forest with satellite thermal sensing and boundary-layer soundings, *J. Appl. Meteorol.*, 32, 909–917, 1993.
- Chamberlain, A. C., Transport of gases to and from grass and grass-like surfaces, *Proc. R. Soc. London., Ser. A.*, 290, 236–265, 1966.
- Chen, H. S., *Space Remote Sensing Systems*, p. 90, Academic, San Diego, Calif., 1985.
- Daubechies, I., *Ten Lectures on Wavelets, CBMS-NSF Reg. Conf. Ser. Appl. Math.*, vol. 61, 357 pp., Soc. for Ind. and Appl. Math., Philadelphia, Pa., 1992.
- Farge, M., Wavelet transforms and their applications to turbulence, *Annu. Rev. Fluid Mech.*, 24, 395–457, 1992.
- Feijt, A. J., and W. Koshiek, The effect of emissivity variation on surface temperature determined by infrared radiometry, *Boundary Layer Meteorol.*, 72, 323–327, 1995.
- Finnigan, J. J., Turbulence in waving wheat: Mean statistics and homnami, *Boundary Layer Meteorol.*, 16, 181–211, 1979.
- Fisher, M. J., and P.O.A.L. Davies, Correlation measurements in a non-frozen pattern of turbulence, *J. Fluid Mech.*, 18, 97–115, 1964.
- Fuchs, M., Infrared measurement of canopy temperature and detection of plant stress, *Theor. Appl. Climatol.*, 42, 253–261, 1990.
- Hayashi, T., An analysis of wind velocity fluctuations in the atmospheric surface layer using orthonormal wavelet transform, *Boundary Layer Meteorol.*, 70, 307–326, 1994.
- Hogstrom, U., Analysis of turbulence in the surface layer with a modified similarity formulation for near-neutral conditions, *J. Atmos. Sci.*, 47, 1949–1972, 1990.
- Huband, N.D.S., and J. L. Monteith, Radiative surface temperature and energy balance of a wheat canopy, *Boundary Layer Meteorol.*, 36, 1–17, 1986.
- Kader, B. A., and A. M. Yaglom, Mean fields and fluctuation moments in the unstably stratified turbulent boundary layers, *J. Fluid Mech.*, 212, 637–662, 1990.
- Kader, B. A., and A. M. Yaglom, Spectra and correlation functions of surface layer turbulence in unstably stratified thermal stratification, in *Turbulence and Coherent Structures*, edited by O. Metais, and M. Lesieur, pp. 388–412, Kluwer Acad., Norwell, Mass., 1991.
- Kaimal, J. C., and J. J. Finnigan, *Atmospheric Boundary Layer Flows: Their Structure and Measurement*, 289 pp., Oxford Univ. Press, New York, 1994.
- Kaneko, D., and M. Hino, Proposal and investigation of a method for estimating surface energy balance in regional forests using TM derived vegetation index and observatory routine data, *Int. J. Remote Sens.*, 17, 1129–1148, 1996.
- Katul, G. G., and M. B. Parlange, Estimation of bare soil evaporation using skin temperature measurements, *J. Hydrol.*, 132, 91–106, 1992.
- Katul, G. G., and M. B. Parlange, On the active role of temperature in surface layer turbulence, *J. Atmos. Sci.*, 51, 2181–2195, 1994.
- Katul, G. G., and M. B. Parlange, Analysis of land surface heat fluxes using the orthonormal wavelet approach, *Water Resour. Res.*, 31, 2743–2749, 1995.
- Katul, G. G., and B. Vidakovic, The partitioning of attached and detached eddy motion in the atmospheric surface layer using Lorentz wavelets, *Boundary Layer Meteorol.*, 77, 153–172, 1996.
- Katul, G. G., J. D. Albertson, C. R. Chu, and M. B. Parlange, Intermittency in atmospheric surface layer turbulence: The orthonormal wavelet representation, in *Wavelets in Geophysics*, edited by E. Foufoula-Georgiou and P. Kumar, pp. 81–105, Academic, San Diego, Calif., 1994.
- Katul, G. G., S. M. Goltz, C. I. Hsieh, Y. Cheng, F. Mowry, and J. Sigmon, Estimation of surface heat and momentum fluxes using the flux-variance method above uniform and non-uniform terrain, *Boundary Layer Meteorol.*, 74, 237–260, 1995.
- Katul, G. G., P. L. Finkelstein, J. F. Clarke, and T. G. Ellestad, An investigation of the conditional sampling method used to estimate fluxes of active, reactive, and passive scalars, *J. Appl. Meteorol.*, 35, 1835–1845, 1996a.
- Katul, G. G., J. D. Albertson, C. I. Hsieh, P. S. Conklin, J. T. Sigmon, M. B. Parlange, and K. R. Knoerr, The inactive eddy motion and the large-scale turbulent pressure fluctuations in the dynamic sublayer, *J. Atmos. Sci.*, 53, 2512–2524, 1996b.
- Kolmogorov, A. N., The local structure of turbulence in incompressible viscous fluid for very large Reynolds numbers, *Dokl. Akad. Nauk SSSR*, 30, 301–304, 1941.
- Koshiek, W., H.A.R. De Bruin, H. The, and B. Van den Hurk, Estimation of the sensible heat flux of a semi-arid area using radiative temperature measurements, *Boundary Layer Meteorol.*, 63, 213–230, 1993.
- Kumar, P., and E. Foufoula-Georgiou, Wavelet analysis in geophysics: An introduction, in *Wavelets in Geophysics*, edited by E. Foufoula-Georgiou and P. Kumar, pp. 1–43, Academic, San Diego, Calif., 1994.
- Lagouarde, J. P., and Y. Kerr, Experimental study of angular effects on brightnear surface temperature for various types of surfaces, in *Thermal Remote Sensing of the Energy and Water Balance over Vegetation in Conjunction with other Sensors, ACTES Proceedings*, pp. 107–111, Cemagref-Engref, Montpellier, France, 1993.
- Lumley, J. L., Interpretation of time spectra measured in high intensity shear flows, *Phys. Fluids*, 8, 1056–1062, 1965.
- Massman, W. J., Heat transfer to and from vegetated surfaces: An analytical method for bulk exchange coefficients, *Boundary Layer Meteorol.*, 40, 269–281, 1987.
- Mathur, A. K., S. Ilanthirayan, and V. K. Agarwal, Instantaneous near-surface level humidity from ERS-1/ATSR observations: A case study in the Indian Ocean, *Int. J. Remote Sens.*, 17, 771–781, 1996.
- Meneveau, C., Analysis of turbulence in the orthonormal wavelet representation, *J. Fluid Mech.*, 224, 429–484, 1991a.
- Meneveau, C., Dual spectra and mixed energy cascade of turbulence in the wavelet representation, *Phys. Rev. Lett.*, 66, 1450–1452, 1991b.
- Mizuno, T., and H. A. Panofsky, The validity of Taylor's hypothesis in the atmospheric surface layer, *Boundary Layer Meteorol.*, 9, 375–380, 1975.
- Monin, A. S., and A. M. Obukhov, Basic laws of turbulent mixing in the ground layer of the atmosphere, *Tr. Geofiz. Inst. Akad. Nauk SSSR*, 24, 163–187, 1954.
- Owen, P. R., and W. R. Thomson, Heat transfer across surfaces, *J. Fluid Mech.*, 15, 321–334, 1963.
- Panofsky, H. A., and J. A. Dutton, *Atmospheric Turbulence*, 397 pp., John Wiley, New York, 1984.
- Perry, A. E., S. Henbest, and M. S. Chong, A theoretical and experimental study of wall turbulence, *J. Fluid Mech.*, 165, 163–199, 1986.
- Powell, D., and C. E. Elderkin, An investigation of the application of Taylor's hypothesis to atmospheric boundary turbulence, *J. Atmos. Sci.*, 31, 990–1002, 1974.
- Qualls, R. J., and W. Brutsaert, Evaluation of spatially distributed ground-based and remotely sensed data to estimate spatially distributed sensible heat fluxes, *Water Resour. Res.*, 32, 2489–2495, 1996.
- Raupach, M. R., Conditional statistics of Reynolds stress in rough-wall and smooth-wall turbulent boundary layers, *J. Fluid Mech.*, 108, 363–382, 1981.
- Raupach, M., R. Antonia, and S. Rajagopalan, Rough-wall turbulent boundary layers, *Appl. Mech. Rev.*, 44, 1–25, 1991.
- Raupach, M. R., J. J. Finnigan, and Y. Brunet, Coherent eddies and turbulence in vegetation canopies: The mixing-layer analogy, *Boundary Layer Meteorol.*, 78, 351–382, 1996.
- Sugita, M., and W. Brutsaert, Landsat surface temperatures and radiosoundings to obtain regional surface fluxes, *Water Resour. Res.*, 28, 1675–1679, 1992.
- Sugita, M., and W. Brutsaert, Optimal measurement strategy for surface temperature to determine sensible heat flux from anisothermal vegetation, *Water Resour. Res.*, 32, 2129–2134, 1996.
- Sugita, M., and A. Kubota, Radiometrically determined skin temperature and scalar roughness to estimate surface heat flux, II, Performance of parameterized scalar roughness for the determination of sensible heat, *Boundary Layer Meteorol.*, 70, 1–12, 1994.
- Szilgayi, J., G. G. Katul, M. B. Parlange, J. D. Albertson, and A. T. Cahill, The local effect of intermittency on the inertial subrange energy spectrum of the atmospheric surface layer, *Boundary Layer Meteorol.*, 79, 35–50, 1996.
- Taylor, G. I., The spectrum of turbulence, *Proc. R. Soc. London, Ser. A*, 164, 476–490, 1938.

- Tennekes, H., Similarity relations, scaling laws and spectral dynamics, in *Atmospheric Turbulence and Air Pollution Modelling*, edited by F.T.M. Nieuwstadt and H. van Dop, pp. 37–68, D. Reidel, Norwell, Mass., 1973.
- Townsend, A. A., Equilibrium layers and wall turbulence, *J. Fluid Mech.*, 128, 283–332, 1961.
- Townsend, A. A., *The Structure of Turbulent Shear Flows*, 429 pp., Cambridge Univ. Press, New York, 1976.
- Vining, R. C., and B. L. Blad, Estimation of sensible heat flux from remotely sensed canopy temperatures, *J. Geophys. Res.*, 97, 18951–18954, 1992.
- Yaglom, A. M., Fluctuation spectra and variances in convective turbulent boundary layers: A reevaluation of old models, *Phys. Fluids*, 6, 962–972, 1994.
- Yaglom, A. M., and B. A. Kader, Heat and mass transfer between a rough wall and turbulent fluid flow at high Reynolds and Peclet numbers, *J. Fluid Mech.*, 62, 601–623, 1974.
- Yamada, M., and K. Ohkitani, Orthonormal wavelet expansion and its application to turbulence, *Prog. Theor. Phys.*, 86, 819–823, 1990.
- Yamada, M., and K. Ohkitani, Orthonormal wavelet analysis of turbulence, *Fluid Dyn. Res.*, 8, 101–115, 1991a.
- Yamada, M., and K. Ohkitani, An identification of energy cascade in turbulence by orthonormal wavelet analysis, *Prog. Theor. Phys.*, 86, 799–815, 1991b.

C.-I. Hsieh and G. G. Katul, School of the Environment, Box 90328, Duke University, Durham, NC 27708-0328. (e-mail: hsieh@acpub.duke.edu; gaby@duke.edu)

J. Schieldge, Jet Propulsion Laboratory, California Institute of Technology, Pasadena, CA 91109-8099. (e-mail: john@lithos.jpl.nasa.gov)

B. Vidakovic, Institute of Statistics and Decision Sciences, Duke University, Durham, NC 27708. (e-mail: brani@stat.duke.edu)

(Received October 21, 1997; accepted January 23, 1998.)